JOURNAL OF GEOPHYSICAL RESEARCH, VOL. 112, B05206, doi:10.1029/2006JB004546, 2007

Vibrational and thermodynamic properties of forsterite at mantle conditions

Li Li,[1] Renata M. Wentzcovitch,[2] Donald J. Weidner,[1] and Cesar R. S. Da Silva[2]

Received 5 June 2006; revised 6 November 2006; accepted 15 January 2007; published 9 May 2007.

[1] We present a first-principle study of the vibrational and thermodynamic properties of Mg_2SiO_4 forsterite up to 20 GPa. The calculated local density approximation (LDA) frequencies and their pressure dependence are in good agreement with the available Raman and infrared spectroscopy data. We also predict the pressure dependence of the modes which are yet to be measured. Thermodynamic properties are obtained using the quasi-harmonic approximation (QHA) to the free energy in conjunction with these results. The calculated pressure-volume-temperature (P-V-T) relations and thermodynamic properties agree well with the reported experimental data within the regime of validity of the QHA. The only discrepancies with experimental data that point to intrinsic anharmonic effects are the mode Gruneisen parameters of two Raman and one infrared modes. However, their effect on thermodynamic properties appears to be negligible.

Citation: Li, L., R. M. Wentzcovitch, D. J. Weidner, and C. R. S. Da Silva (2007), Vibrational and thermodynamic properties of forsterite at mantle conditions, *J. Geophys. Res.*, *112*, B05206, doi:10.1029/2006JB004546.

1. Introduction

[2] Mg_2SiO_4 forsterite is the end-member of olivine, which is the major constituent of the upper mantle. It has been widely studied; the results can be seen in both vibrational spectroscopy [*Akaogi et al.*, 1984; *Chopelas*, 1990; *Ghose et al.*, 1992; *Gillet et al.*, 1991; *Hofmeister*, 1987; *Iishi*, 1978; *Pilati et al.*, 1995; *Rao et al.*, 1988; *Wang et al.*, 1993] and elasticity measurements [*Cynn et al.*, 1998; *Downs et al.*, 1996; *Duffy et al.*, 1995; *Guyot et al.*, 1996; *Isaak et al.*, 1989; *Li et al.*, 1996; *Meng et al.*, 1993; *Zha et al.*, 1994]. Vibrational modes of forsterite measured at high pressure in the laboratory are limited in its number of detected modes (84 modes for forsterite in total) even though the stability of forsterite reaches 410 km depth of the Earth. Previous lattice dynamic calculations [*Pavese*, 1998; *Price et al.*, 1987] on forsterite are limited to the usage of empirical potentials. The first-principles approach based on density functional theory [*Hohenberg and Kohn*, 1964] has been successfully applied to predict the structural and elastic properties of Mg_2SiO_4 forsterite at high pressures [*da Silva et al.*, 1997; *Wentzcovitch and Stixrude*, 1997], while the vibrational properties are yet to be explored with this approach.

[3] In the past decade, first-principles lattice dynamics in conjunction with the quasi-harmonic approximation (QHA) has been applied to predict vibrational and thermodynamic properties of mantle minerals such as MgO pericalse [*Karki et al.*, 2000c], $MgSiO_3$ perovskite [*Karki et al.*, 2000b], $MgSiO_3$ ilmenite [*Karki et al.*, 2000a], $MgSiO_3$ postperovskite [*Tsuchiy et al.*, 2004; *Tsuchiya et al.*, 2005], and Mg_2SiO_4 ringwoodite [*Yu and Wentzcovitch*, 2006] at mantle conditions. The predicted vibrational and thermoelastic properties of these minerals and their aggregates have been reported to be in very good agreement with available experimental data and preliminary reference Earth model (PREM). Now we address the properties of Mg_2SiO_4 forsterite with the same methods. In contrast, with these other minerals, Mg_2SiO_4 forsterite is stable at lower pressures up to 14 GPa. Some studies have reported anharmonic characteristics in forsterite [*Anderson*, 1996; *Cynn et al.*, 1996; *Gillet et al.*, 1991] based on the observation of the temperature dependence of the Raman and acoustic frequencies, in addition to thermodynamic considerations by which C_V was determined from measurements of C_P. Here we will compare the calculated and measured vibrational properties of forsterite and investigate the validity of the QHA formulation to reproduce its thermodynamic properties.

2. Method

[4] Our computations use the local density approximation (LDA) [*Celperley and Alder*, 1990; *Perdew and Zunger*, 1981]. Calculation details are similar to those reported in previous works [*Karki et al.*, 2000b; *Tsuchiy et al.*, 2004; *Tsuchiya et al.*, 2005; *Yu and Wentzcovitch*, 2006]. The equilibrated structure of forsterite was calculated using the first-principles implementation of a variable cell-shape damped molecular dynamics (VCSMD) [*Wentzcovitch and Price*, 1996; *Wentzcovitch et al.*, 1995]. Pseudopotentials of Mg were generated by the method of von Barth and Car [*Karki et al.*, 2000b;

---

[1] Department of Geosciences, Mineral Physics Institute, Stony Brook University, Stony Brook, NY, USA.

[2] Department of Chemical Engineering and Materials Science, Minnesota Supercomputing Institute for Digital Technology and Advanced Computations, University of Minnesota, Minneapolis, MN, USA.

0148-0227/07/2006JB004546$09.00

Tsuchiya et al., 2005], while those of O and Si are by the method of Troullier and Martins [*Troullier and Martins*, 1991]. The plane wave energy cut-off used is 70 Ry, and the *k* point sampling of the charge density was performed on a 2 × 2 × 2 grid in Brillouin zone (BZ) shifted by $^1/_2,^1/_2,^1/_2$The calculations with 2 × 2 × 2 and 4 × 2 × 4 grid of *k* points give a difference in energy by 0.1 meV/atom, in pressure by 0.03 GPa. Thus using 4 × 2 × 4 grid changes little on the precision for this study. The dynamical matrix was obtained using density functional perturbation theory (DFPT) [*Baroni et al.*, 2001]. At each pressure, dynamical matrices were calculated on a 2 × 2 × 2 (without shift) *q* point mesh; force constants were extracted and used to produce matrices in a 12 × 12 × 12 *q* point grid. The corresponding normal modes were used in the calculation of the free energy.

3. Results and Discussion

[5] Forsterite has an orthorhombic structure (Pbnm, $Z = 4$). Mg atoms occupy two distinct octahedral sites: M1 (4a) and M2 (4c); Si atoms occupy the tetrahedral site (4c); O atoms occupy three distinct sites at tetrahedral corners: O1 (4c), O2 (4d), and O3 (8d). The oxygen atoms form a distorted hexagonal close-packed arrangement. The unit cell has four formulas (28 atoms), so there are 84 vibrational modes at each *q* point in the Brillouin zone, among which 3 are acoustic and 81 are optical modes. The irreducible representation of forsterite lattice at the BZ center is as in equation (4a)

$$\begin{aligned}\Gamma_{op} = {} & 11A_g + 7B_{1g} + 11B_{2g} \\ & + 7B_{3g} + 10A_u + 14B_{1u} + 10B_{2u} + 14B_{3u}\end{aligned} \tag{4a}$$

where $11A_g + 7B_{1g} + 11B_{2g} + 7B_{3g}$ are Raman active; $14B_{1u} + 10B_{2u} + 14B_{3u}$ are infrared active; and $10A_u$ is inactive. The three acoustic modes are $B_{1u} + B_{2u} + B_{3u}$.

[6] The calculated phonon dispersion along several symmetry directions and the vibrational density of states at 0 and 20 GPa are shown in Figure 1. The diagonal components of the dielectric tensor are (2.85, 2.77, 2.79) at zero pressure and (2.87, 2.78, 2.79) at 20 GPa. The Born effective charges of Mg are close to 2 for Mg, while those for Si and O are significantly different from ideal values of 4 and −2 and are highly anisotropic. For Mg, they are Z*[Mg] = (2.17, 1.72, 1.94) at 0 Gpa and (2.11, 1.71, 1.89) at 20 GPa; Z*[Si] = (3.07, 2.62, 2.92) at 0 GPa and (3.10, 2.74, 2.99) at 20 GPa; Z*[O1] = (−2.33, −1.40, −1.47) and Z*[O2] = (−1.60, −1.98, −1.53) at 0 GPa, and Z*[O1] = (−2.27, −1.42, −1.49) and Z*[O2] = (−1.58, −1.61, −1.85) at 20 GPa.

[7] We list our calculated frequencies of the optical Raman modes at 0 GPa and 0 K in Table 1, infrared modes in Table 2, and inactive modes at zone center in Table 3 and compare these with previously reported results at 0 GPa pressure. Also, listed are the mode Grüneisen parameters ($\gamma_i = -d(ln\omega_i)/dlnV$). A number of studies have reported the phonon frequencies of forsterite at zero pressure using different techniques such as Raman and infrared spectroscopy [e.g., *Iishi*, 1978; *Lam et al.*, 1990] and inelastic neutron scattering [*Rao et al.*, 1988]; only the results from one study [*Iishi*, 1978] are listed in Tables 1 and 2, since these studies agree well with each other. The frequency of an infrared active mode splits into two values depending on whether the mode is longitudinal (LO) or transverse (TO), which is due to the contribution of the macroscopic electric field to the LO mode in a polar crystal. The calculated eigenvectors, which contain information about the internal and external motions of the SiO_4 tetrahedral and Mg ions, are used to deduce the symmetry labels of the modes following a method described elsewhere [*Rao et al.*, 1988]. We find similar frequency-pressure relationships between Raman and infrared modes. The calculated frequencies at the zone center are all positive and increase with pressure for Raman (Figure 2a) and infrared modes alike (Figure 2b). The pressure dependences of mode frequencies are consistent with available experimentally fitted curves [*Chopelas*, 1990; *Hofmeister*, 1987; *Wang et al.*, 1993]. Only two Raman modes, the lowest B_{3g} ones and one B_{1u} IR mode, have the calculated γ_i considerably different from measured ones. This might be signs of forsterite's anharmonicity, not properly accounted for by the present approach.

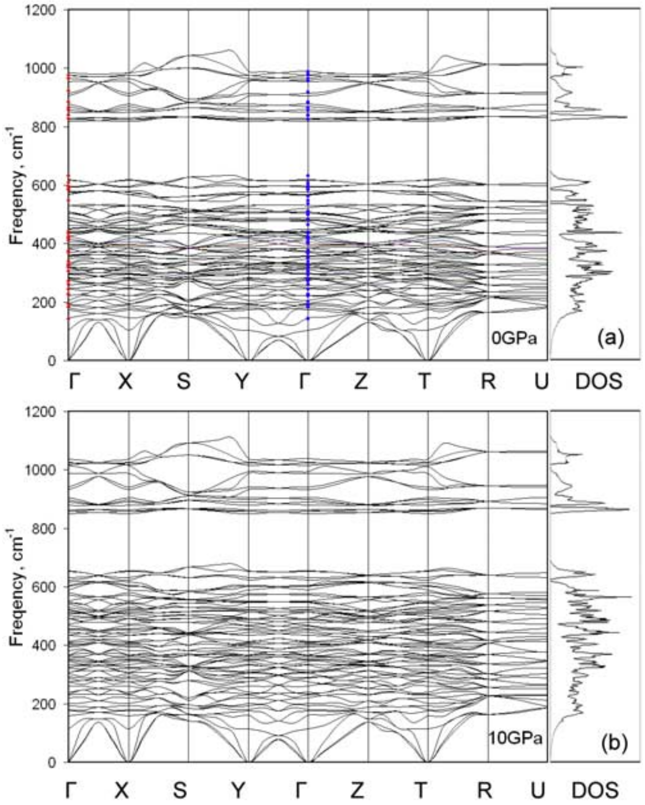

Figure 1. Phonon dispersion and vibrational density of states of Mg_2SiO_4 forsterite, (a) 0 GPa and (b) 20 GPa. The infrared and Raman spectra are plotted as red dots [*Iishi*, 1978] and blue dots [*Lam et al.*, 1990], respectively. The points in the Brillouin zone are Ã = (0, 0, 0); X = (0, 0, 2π/a); S = (π/a, π/b, 0); Y = (0, 2π/b, 0); Z = (0, 0, π/c); T = (0, 2π/b, π/c); R = (π/a, π/b, π/c); and U = (π/a, 0, π/c).

Table 1. Vibrational Raman Modes of Forseterite at Ambient Conditions in cm^{-1}

	Calculation		Experiment					
			υ_i		γ_i			
	υ_I	γ_i	a,b	c	c	d	e	Modes Type[a]
A_g	188	0.30	183					T′(Mg2, SiO4:x)
	222	0.75	227	227	0.70	0.64	0.67	T′(SiO4, Mg2:y)
	316	1.21	305	306	1.80	1.36	1.63	T′(Mg2, SiO4:x)
	333	1.21	329					T′(Mg2, SiO4:x)
	357	1.19	340	341		1.78	1.87	R′(SiO4:z)
	436	1.36	424					$\upsilon 2$
	529	0.77	546					$\upsilon 4$
	596	0.69	609	609	0.70	0.68	0.70	$\upsilon 4$
	818	0.46	826	826	0.50	0.48	0.48	$\upsilon 1$
	850	0.42	856	856	0.50	0.43	0.49	$\upsilon 3$
	965	0.59	965					$\upsilon 3$
B_{3g}	195	1.11	226	183		2.15	2.09	T′(SiO4:z)
	284	0.73	272	290		1.35		T′(Mg2:z)
	320	1.07	318					R′(SiO4:y)
	383	0.94	376					R′(SiO4:z)
	418	1.14	412	424		0.97	0.99	$\upsilon 2$
	577	0.58	595	587		0.61		$\upsilon 4$
	914	0.36	922	922	0.40	0.38	0.38	$\upsilon 3$
B_{2g}	174	0.09	142					T′(Mg2,z)
	249	1.07	244	244		1.23	1.21	T′(SiO4:z)
	329	1.24	324					R′(SiO4:x)
	370	1.04	368	376	1.40	1.26	1.25	R′(SiO4:y)
	450	1.27	441	441	1.80	1.59	1.60	$\upsilon 2$
	568	0.57	588	545	0.60	0.42	0.53	$\upsilon 4$
	877	0.40	884	884	0.50	0.44	0.44	$\upsilon 3$
B_{1g}	222	0.81	192	227	0.70	0.64	0.67	T′(Mg2:SiO4:y)
	256	0.94	224					T′(Mg2:SiO4:x)
	327	1.20	260					T′(Mg2:SiO4:x)
	360	1.16	318	331	1.30	1.14	1.12	T′(Mg2:y)
	384	0.90	418					R′(SiO4:z)
	444	1.23	434	434		1.35	1.40	$\upsilon 2$
	569	0.61	583	584	0.60	0.48	0.66	$\upsilon 4$
	618	0.68	632					$\upsilon 4$
	829	0.48	839	826	0.50	0.48	0.48	$\upsilon 1$
	858	0.40	866	856	0.50	0.43	0.49	$\upsilon 3$
	975	0.59	976	966	0.70	0.66	0.66	$\upsilon 3$

[a] The assignments follow a previous study [*Iishi*, 1978]. R (rotational lattice mode) and T (translational lattice modes) are the two external modes. The four internal vibrational modes of SiO4 ion are υ_1(A1 type), υ_2(E type), υ_3, and υ_4 (F2 type). References: a, [*Iishi*, 1978]; b, [*Lam et al.*, 1990]; c, [*Gillet et al.*, 1991]; d, [*Wang et al.*, 1993]; and e, [*Chopelas*, 1990]. v_i is the vibrational frequency; γ_i is the Grüneisen parameter of mode i as defined in equation 5b.

Table 2. Calculated Frequencies (cm^{-1}) of Infrared Modes of Forsterite, Compared With Experiments at Zero Pressure[a]

	Calculation			Experiment						
				υ_{TO}	υ_{LO}	υ_i	γ_i	υ_i	γ_i	
	υ_{TO}	υ_{LO}	γ_i	a	a	b	b	c	c	Mode Type[a]
B_{3u}	205	205	1.16	201						T′(Mg1, SiO4:y)
	277	277	0.57	224						T′(Mg2:x,y)
	296	297	1.04	274	276					T′(Mg1:x; Mg2:y)
	321	323	1.12	293	298					T′(Mg1:x,z)
	398	403	1.13	320	323					T′(Mg1:z,y)
	407	450	1.07	378	386					T′(Mg2:x,y)
	482	482	1.00	403	469					R′(SiO4:x)
	508	520	0.89	498	544					$\upsilon 2$
	531	532	0.86	562	566					$\upsilon 4$
	593	606	0.61	601	645					$\upsilon 4$
	824	825	0.48	838	845	846	0.39	836	0.47	$\upsilon 1$
	954	965	0.41	957	963	962	0.32	925	0.23	$\upsilon 3$
	975	1024	0.61	980	1086					$\upsilon 3$
B_{2u}	146	146	1.06	144						T1(Mg1:SiO4:x)
	282	284	0.80	224						T;(Mg2:x)
	295	307	0.74	280	283					T′(Mg1:y)
	363	376	1.27	294	313					T′(Mg1:x,z; Mg2:y)
	398	419	1.11	352	376					T′(Mg2:x,y)
	427	430	1.20	400	412					T′(Mg1:z)
	463	472	1.14	421	446					R′(SiO4:z)
	502	507	0.74	465	493					$\upsilon 2$
	530	532	0.86	510	516					$\upsilon 4$
	617	617	0.66	537	597	614	0.54	609	0.28	$\upsilon 4$
	825	830	0.48	838	843					$\upsilon 1$
	868	914	0.43	882	979					$\upsilon 3$
	985	986	0.59	987	993	992	0.65	988	0.68	$\upsilon 3$
B_{1u}	194	194	0.63	201						T′(Mg1:y,z)
	278	279	0.57	224						T′(Mg1:x)
	296	304	0.81	274	278					T′(Mg1:y; Mg2:z)
	316	317	1.11	296	318					T′(Mg1:z)
	426	438	1.24	365	371					R′(SiO4:z)
	428	443	1.38	423	459					R′(SiO4:y)
	475	490	0.96	483	489					$\upsilon 2$
	504	518	0.87	502	585	517	0.50	483	0.38	$\upsilon 4$
	870	931	0.40	885	994	887	0.39	876	0.32	$\upsilon 3$

[a] The assignments follow a previous study [*Iishi*, 1978]. R (rotational lattice mode) and T (translational lattice modes) are the two external modes. The four internal vibrational modes of SiO4 ion are υ_1(A1 type), υ_2(E type), υ_3 and υ_4 (F2 type). References: a, [*Iishi*, 1978]; b, [*Wang et al.*, 1993]; c, [*Hofmeister*, 1987]. v_i is the vibrational frequency; γ_i is the Grüneisen parameter of mode i as defined in equation 5b.

However, their effect on thermodynamics properties seems to be unnoticeable within the regime of validity of the QHA.

4. Thermodynamic Properties

[8] In the QHA formulation, the Helmholtz free energy can be expressed as:

$$F(V,T) = U_0(V) + \frac{1}{2}\sum_{q,j} h\omega_j(q,V) + k_B T \sum_{q,j} \times \ln\left\{1 - \exp\left[-h\omega_j(q,V)/k_B T\right]\right\} \tag{4b}$$

where the first term is the internal energy, the second is the zero point motion energy, and the third is the vibrational energy contribution, where ω_j represents phonons with normal mode q. The total vibrational energy of a crystal is the sum over all the phonon modes in the Brillouin zone. In our calculation, the sum is performed on a 12 × 12 × 12 q mesh, i.e., 343 unequivalent points in the first BZ. When comparing predictions of the QHA with measurements, it is important to be aware of the domain of validity of this

Table 3. Calculated Frequencies (cm^{-1}) and Mode Grüneisen Parameters for A_u Inactive Modes at Zero Pressure

υ_i	υ_i[a]	γ_i
104	171	0.98
180	161	0.16
246	225	0.69
299	286	1.17
348	347	1.08
390	376	1.17
439	437	1.31
480	469	0.95
509	511	0.86
905	885	0.37

[a] [*Lam et al.*, 1990].

approximation [*Gillet et al.*, 1997; *Stacey and Isaak*, 2003]. The maximum temperature at which the QHA is predictive at a particular pressure can be inferred from a posteriori inspection of the thermal expansion coefficient, $\alpha(T)$. There is, in general, a deviation from the linearity of $\alpha(T)$ at high T, i.e., at some T between the Debye temperature (~750°C) and the melting temperature (~2160°C); the zero point of $\partial^2\alpha/\partial T^2$ can be used to bind the QHA validity region (*Wentzcovitch et al.*, 2004). Using this criterion, our results indicate that QHA is valid for forsterite in the upper mantle (Figure 3). In the following, we present our results and compare them with experimental data, from which we can see the effectiveness of the QHA. The results at pressure and temperature regions (P-Ts) where the QHA is valid are plotted as solid line, otherwise plotted as dotted line. Differences between calculations and measurements can also be seen in the QHA invalid P-T region. Although we have not done so, anharmonicity in this P-T domain could perhaps be accounted for by introducing in equation (4b) a term of $a_v K_B T^2$ where $a_v = (\partial \ln v/\partial T)v$ defined by *Downs et al.* [1996], *Gillet et al.* [1991], and *Guyot et al.* [1996]. There are limited data a_v available; only 20 out of 81 modes have been reported [*Downs et al.*, 1996; *Gillet et al.*, 1991; *Guyot et al.*, 1996], thus it is difficult to apply this procedure to this study.

[9] The calculated pressure-volume-temperature (P-V-T) relations are plotted in Figure 4. These curves are fitted with isothermal third-order finite strain equations [*Birch*, 1986] yielding $V_0 = 289.5$ Å^3, $K_0 = 126.4$ GPa, $\hat{E}_0 = 4.2$. These compression curves are in good agreement with the experimental data [*Downs et al.*, 1996; *Gillet et al.*, 1991, *Meng et al.*, 1993, 106; *Guyot et al.*, 1996]. A comparison of calculated and measured thermodynamic properties at room temperature and pressure is reported in Table 4. The agreement between calculated and measured values is excellent.

[10] In Figures 5a–5g, the calculated thermodynamical properties are plotted and compared with reported data as a function of pressure and temperature. The isothermal

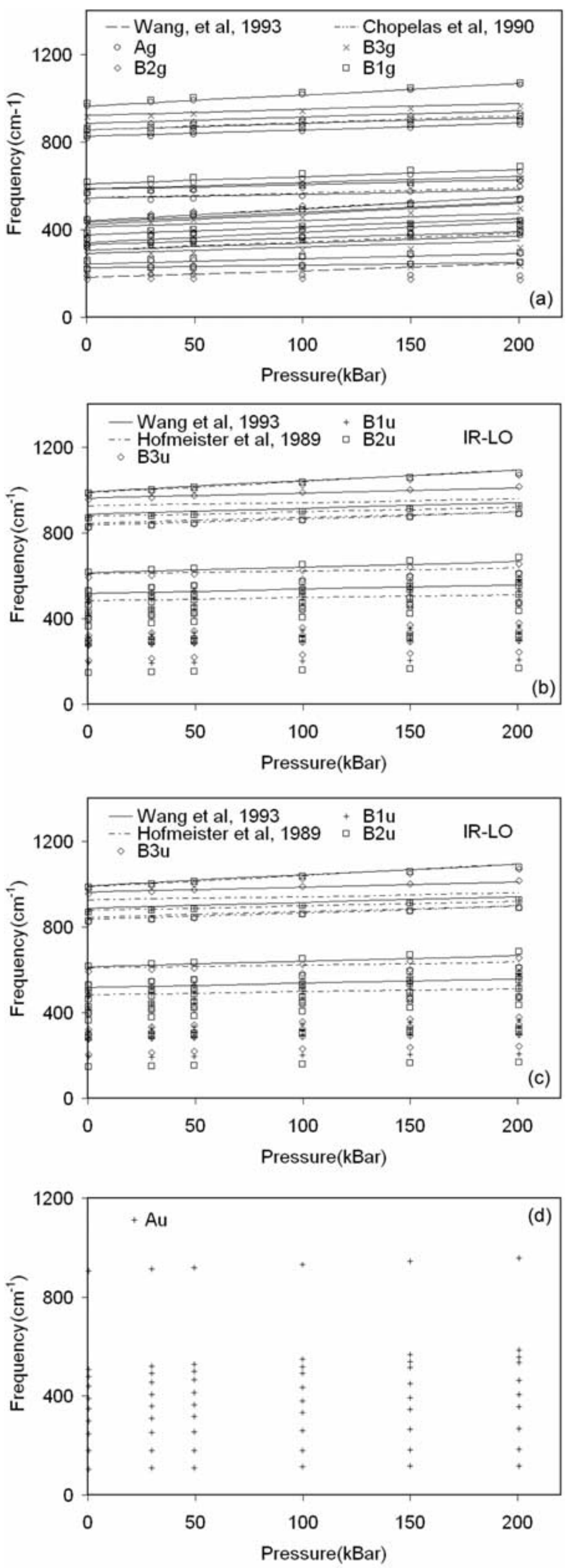

Figure 2. Pressure dependence of the frequencies of (a) Raman vibrational modes, (b) infrared TO, (c) infrared LO, and (d) inactive mode at the zone center. Cross symbols are calculated frequencies. The solid line and dashed line are experimentally extrapolated results.

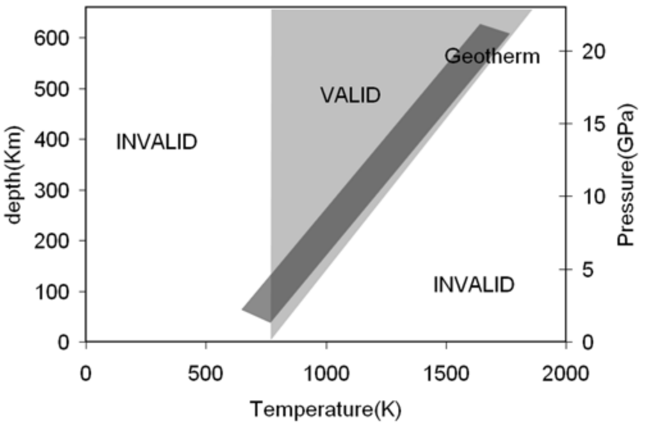

Figure 3. The valid pressure and temperature region of QHA estimated from calculated thermal expansion coefficient. The thick line indicates an estimate of geotherm [*Brown and Shankland*, 1981; *Green et al.*, 1999], the light gray region is the QHA valid region.

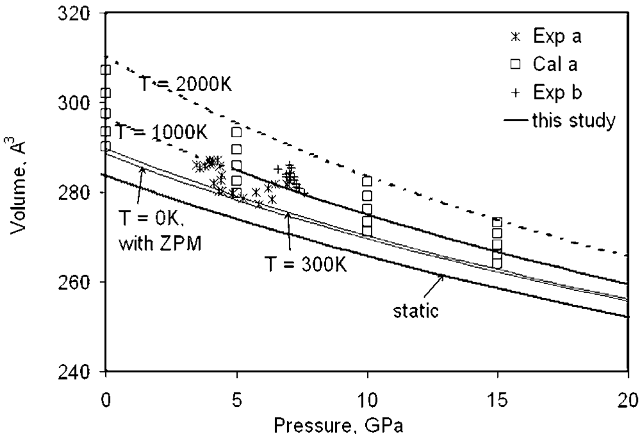

Figure 4. Calculated pressure-temperature-volume relations for forsterite. "Static" represents the results for static lattice (without zero point motion). "T = 0K, with ZPM" represents the results after the zero point motion correction. "Exp a" represents the measured data in the temperature range 675–1273 K by *Guyot et al.* [1996]; "Cal a" is the calculated values at 300 K, 700 K, 1100 K, 1500 K, and 1900 K using QHA by *Guyot et al.* [1996]. "Exp b" represents the measured data in the temperature range 1019–1371 K by *Meng et al.* [1993]. Solid black lines are calculated results at P-T where QHA is valid; dashed lines extended beyond the solid are at P-T condition where QHA is invalid.

(K_T) and adiabatic (K_S) bulk modulus are plotted in Figures 5a and b. Our K_Ts are in excellent agreement with experimental values at 0 GPa [*Gillet et al.*, 1991] and so is $K_S = K_T(1 + \alpha\gamma T)$ within the regime of validity of the QHA [*Gillet et al.*, 1991 ; *Isaak et al.*, 1989]. Figure 5c shows the thermal expansivity, $\alpha = \frac{1}{V}\left[\frac{\partial V}{\partial T}\right]_P$, which is determined from the volume dependence of temperature at each pressure. The scattering of experimental data [*Bouhifd et al.*, 1996; *Chopelas*, 1990; *Fei and Saxena*, 1987; *Gillet et al.*, 1991; *Hazen*, 1976; *Kajiyoshi*, 1986; *Suzuki et al.*, 1984] is substantial at high temperatures even at 0 GPa. Nevertheless, our results are in very good agreement with experimental data within the range of validity of the QHA. At higher pressure, the effect of anharmonicity caused by temperature is expected to decrease. The estimated thermal expansivity at 10 GPa by *Guyot et al.* [1996] is in excellent agreement with our predictions even beyond the QHA permitted region. Below 1000 K, the differences at 10 GPa are probably due to usage of a less than suitable functional form for $\alpha(T)$ to fit experimental data.

[11] In the QHA, Grüneisen parameters γ_{th} and γ_m derived from equations (5a) and (5b), are equal.

$$\gamma_{th} = \frac{\alpha K_T V}{C_V} \tag{5a}$$

$$\begin{aligned} \gamma_m &= \Sigma(\gamma_i C_{Vi})/\Sigma C_{Vi} \\ \gamma_i &= -(\partial \ln(\omega_i)/\partial \ln V)_T \\ C_{Vi} &= k(h\nu_i/kT)^2 \exp(h\nu_i/kT)/[\exp(h\nu_i/kT) - 1]^2 \end{aligned} \tag{5b}$$

where C_V is the heat capacity at constant volume. ω_i is the phonon frequency of a vibrational mode i; C_{Vi} is the Einstein heat capacity, and γ_i is the mode Grüneisen parameter of mode i; γ_m is defined as Grüneisen parameter in terms of the vibrational modes. The comparison between γ_{th} and γ_m for major earth minerals are explicitly discussed in two other studies [*Anderson*, 1989; *Chopelas*, 2000]. The discrepancies between γ_{th} and γ_m exist in most minerals such as forsterite, ringwoodite, modified spinel, and MgO. Previously reported Raman spectroscopic measurements [*Gillet et al.*, 1991] have demonstrated that the value of γ_m derived from equation (5b) is too small compared to reported γ_{th} derived from equation (5a) [*Chopelas*, 1990], which may be due to intrinsic anharmonic contribution. An intrinsic temperature dependence of some vibrational frequencies appears to have been observed at 0 GPa [*Gillet et al.*, 1991]. In Figure 5d, we show that γ_{th} at ambient conditions predicted by the QHA differs at most by 5% from those inferred from measurements with less thorough sampling of phonon frequencies [*Chopelas*, 1990; *Gillet et al.*, 1991].

Table 4. Calculated Thermal Equation of State Compared With Experimental Data

	300 K, 0 GPa Calculation, This Study	300 K, 0 GPa Experiment	References
V(Å^3)	289.5	291.9	[*Guyot et al.*, 1996]
		290.1	[*Downs et al.*, 1996]
		289.2	[*Gillet et al.*, 1991]
K_T(GPa)	126.4	125(2)	[*Downs et al.*, 1996]
		127.7(2)	[*Gillet et al.*, 1991]
K_T'	4.2	4.0(4)	[*Downs et al.*, 1996]
α($\times$ 10^{-5} K^{-1})	2.64	2.83	[*Bouhifd et al.*,1996]
		2.77	[*Gillet et al.*, 1991]
		2.48	[*Suzuki et al.*, 1984]
		2.56	[*Hazen*, 1976]
		2.72	[*Kajiyoshi*, 1986]
C_P(J mol^{-1} K^{-1})	119.3	117.9	[*Gillet et al.*, 1991]
S(J mol^{-1} K^{-1})	95.9	93.14	[*Chopelas*, 1990]
γth	1.23	1.28	[*Gillet et al.*, 1991]
		1.29	[*Isaak et al.*, 1989]
		1.29	[*Chopelas*, 1990]
K_S(GPa)	127.6	128.8(5)	[*Zha et al.*, 1994]
$\partial K_T/\partial T$($\times$ 10^{-2} GPa K^{-1})	−2.1	−2.1(2)	[*Meng et al.*, 1993]
		−2.0(2)	[*Gillet et al.*, 1991]

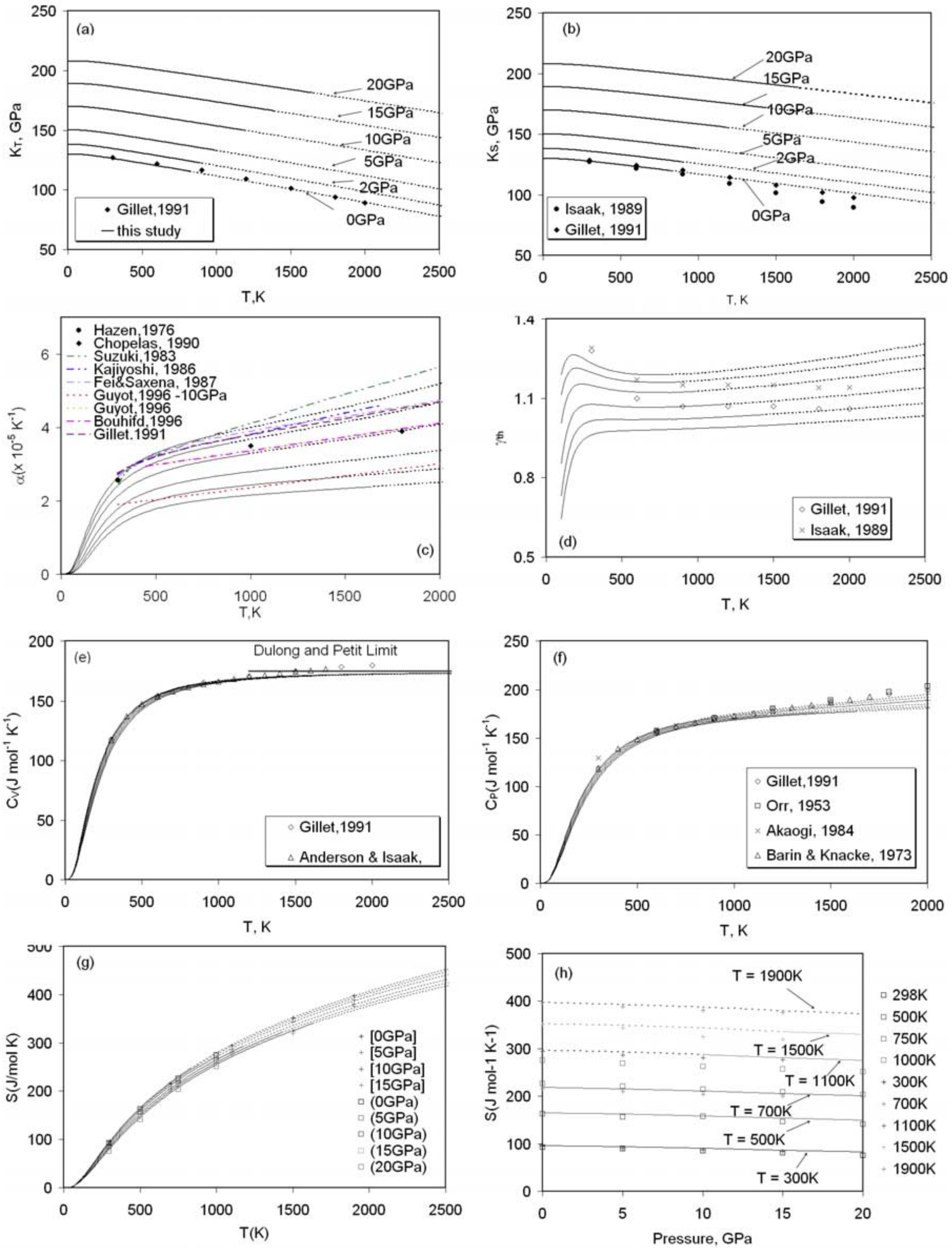

Figure 5. Calculated data at pressure (P = 0, 2, 5, 10, 15, and 20 GPa) and temperature (T). For Figures 5c–5h, the pressure is from 0 GPa to 20 GPa top-down. (a and b) Isothermal (K_T) and adiabatic bulk modulus (K_S); (c) thermal expansivity (α), solid black lines are calculated results at P-T where QHA is valid; dashed lines extended beyond the solid are at P-T condition where QHA is invalid; (d) Grüneisen parameter (γ) compared with reported results [*Gillet et al.*, 1991 ; *Isaak et al.*, 1989]; (e and f) heat capacity C_V and C_P compared with reported results [*Anderson*, 1996; *Gillet et al.*, 1991]; (g and h) entropy (S) versus T and P, cross symbols are by *Guyot et al.* [1996]; square symbols are by *Chopelas* [1990].

[12] A solid is said to be anharmonic in behavior when C_V is larger than that predicted by the Dulong and Petit limit ($3nR$) [*Cynn et al.*, 1996]. Forsterite demonstrates this behavior [*Anderson*, 1996; *Cynn et al.*, 1996; *Gillet et al.*, 1991] at zero pressure and high temperatures. The deviation of our calculated C_V from the experimental results increases with temperature, particularly in the P-T regime where the QHA is no longer expected to be valid. This is the sign of anharmonic effects and is shown in Figure 5e. The difference between calculated and measured C_P, $C_\mathrm{P} = C_\mathrm{V}(1 + \alpha\gamma T)$, is relatively small (Figure 5f). The temperature and pressure dependences of entropy are plotted in Figures 5g–5h. The negative pressure dependences of the entropy at all temperatures are consistent with the experimental results [*Chopelas*, 1990; *Guyot et al.*, 1996]. Our calculated entropy agrees very nicely with the experimental estimates considering the limited number of phonon modes used in the experimental data.

5. Summary

[13] We have reported first-principles phonon dispersion and vibrational density of states for Mg_2SiO_4 forsterite up to 20 GPa using density functional theory. Our calculated Raman and infrared frequencies and their pressure dependences are in excellent agreement with available experimental data. We also predict the pressure dependence of some modes which are yet to be measured. The thermoelastic properties were derived from calculated vibrational density of states (VDoS) in conjunction with the QHA. The calculated compression curves, the isothermal bulk modulus, and the constant pressure-specific heat and entropy agree extremely well with the reported experimental data, regardless of claimed anharmonic effects in this solid. The computed mode Grüneisen parameters, γ_i at zero pressure for three modes, two $B_{3\mathrm{g}}$ and one $B_{1\mathrm{u}}$, differ considerably from measured values, pointing perhaps to the origin of anharmonic effects in this solid. However, the QHA still seems to be very effective in describing thermodynamic, including C_V, properties within its regime of validity. Deviations beyond this limit support the conclusion that forsterite is a solid that is both anharmonic in C_V and quasi-harmonic in the thermal pressure in high-temperature region [*Anderson*, 1996; *Cynn et al.*, 1996 ; *Gillet et al.*, 1991]. The properties of this material at relevant mantle conditions are well predicted by the QHA.

[14] **Acknowledgments.** This research is supported by NSF/EAR 01355, 0230319, NSF/ITR 0428774 (VLAB), and Minnesota Supercomputing Institute. Calculations are performed with Quantum-ESPRESSO package from the Web site http://www.pwscf.org. DJW and LL acknowledge NSF EAR-9909266, EAR0135551, and EAR00135550.

References

Akaogi, M., N. L. Ross, P. McMillan, and A. Navrotsky (1984), The Mg_2SiO_4 polymorphs (olivine, modified spinel and spinel)-thermodynamic properties from oxide melt solution calorimetry phase relations and models of lattice vibrations, *Am. Mineral.*, *69*, 499–512.

Anderson, D. L. (1989), *Theory of the Earth*, Blackwell Sci., Malden, Mass.

Anderson, O. L. (1996), Anharmonicity of forsterite and thermal pressure of insulators, *Geophys. Res. Lett.*, *23*(21), 3031–3034.

Baroni, S., A. Dal Corso, S. de Gironcoli, and P. Giannozzi (2001), Phonons and related crystal properties from density-functional perturbation theory, *Rev. of Mod. Phys.*, *73*(2), 515 LP–562 LP.

Birch, F. D. (1986), Equation of state and thermodynamic parameters of NaCl to 300 kbar in the high-temperature domain, *J. Geophys. Res.*, *91*, 4949–4954.

Bouhifd, M. A., D. Andrault, G. Fiquet, and P. Richet (1996), Thermal expansion of forsterite up to the melting point, *Geophys. Res. Lett.*, *23*(10), 1143–1146.

Brown, J. M., and T. J. Shankland (1981), Thermodynamic parameters in the Earth as determined from seismic profiles, *Geophys. J. R. Astron. Soc.*, *66*, 579–596.

Celperley, D. M., and B. J. Alder (1990), Ground state of the electron gas by a stochastic method, *Phys. Rev. Lett.*, *45*, 566–569.

Chopelas, A. (1990), Thermal properties of forsterite at mantle pressure derived from vibrational spectroscopy, *Phys. Chem. Miner.*, *17*(2), 149–156.

Chopelas, A. (2000), Thermal expansivity of mantle relevant magnesium silicates derived from vibrational spectroscopy at high pressure, *Am. Mineral.*, *85*, 270–278.

Cynn, H., J. D. Carnes, and O. L. Anderson (1996), Thermal properties of forsterite, including Cv, calculated from KT through the entropy, *J. Phys. Chem. Solids*, *57*, 1593–1599.

Cynn, H., D. G. Isaak, and O. L. Anderson, (1998), Elastic properties of forsterite at high pressure obtained from the high-temperature database, in *Properties of Earth and Planetary Materials at High Pressures and Temperatures, Geophysical Monograph 101*, pp. 345–355, AGU, Washington, D. C.

da Silva, C., L. Stixrude, and R. M. Wentzcovitch (1997), Elastic constants and anisotropy of forsterite at high pressure, *Geophys. Res. Lett.*, *24*(15), 1963–1966.

Downs, R. T., C.-S. Zha, T. S. Duffy, and L. W. Finger (1996), The equation of state of forsterite to 17.2 GPa and effects of pressure media, *Am. Mineral.*, *81*, 51–55.

Duffy, T. S., C. S. Zha, R. T. Downs, H. K. Mao, and R. J. Hemley (1995), Elasticity of forsterite to 16 GPa and the composition of the upper mantle, *Nature*, *378*, 170–173.

Fei, Y., and S. K. Saxena (1987), A thermochemical database for phase equilibria in the system Fe-Mg-Si-O at high pressure and temperature, *Phys. Chem. Miner.*, *13*, 311–324.

Ghose, S., N. Choudhury, S. L. Chaplot, and K. Rao (1992), The phonon density of states and thermodynamic properties of minerals, in *Advances in Physical Geochemistry*, pp. 10,283–10,314, Springer, New York.

Gillet, P., P. Richet, F. Guyot, and G. Fiquet (1991), High-temperature thermodynamic properties of forsterite, *J. Geophys. Res.*, *B 96*, 11,805–11,816.

Gillet, P., I. Daniel, and F. Guyot (1997), Anharmonic properties of Mg2SiO4-forsterite measured from the volume dependence of the Raman spectrum, *Eur. J. Mineral.*, *9*(2), 255–262.

Green, D. H., T. J. Falloon, S. M. Eggins, and G. M. Yaxley (1999), Primary magmas and mantle temperatures, *Eur. J. Mineral.*, *13*, 437–451.

Guyot, F., Y. Wang, P. Gillet, and Y. Ricard (1996), Quasi-harmonic computations of thermodynamic parameters of olivines at high-pressure and high-temperature. A comparison with experiment data, *Phys. Earth Planet. Inter.*, *98*, 17–29.

Hazen, R. M. (1976), Effects of temperature and pressure on the structure of forsterite, *Am. Mineral.*, *61*, 1280–1293.

Hofmeister, A. M. (1987), Single-crystal absorption and reflection infrared spectroscopy of forsterite and fayalite, *Phys. Chem. Miner.*, *14*(6), 499–513.

Hohenberg, P., and W. Kohn (1964), Inhomogeneous electron gas, *Phys. Rev. B*, *136*, 364–871.

Iishi, K. (1978), Lattice dynamics of forsterite, *Am. Mineral.*, *63*, 1198–1208.

Isaak, D. G., O. L. Anderson, T. Goto, and I. Suzuki (1989), Elasticity of single-crystal forsterite measured to 1700 K, *J. Geophys. Res.*, *94*, 5895–5906.

Kajiyoshi, K. (1986), High Temperature Equation of State for Mantle Minerals and Their Anharmonic Properties, Okayama University, Okayama, Japan.

Karki, B. B., W. Duan, C. R. S. d. Silva, and R. M. Wentzcovitch (2000a), Ab initio study of MgSiO3-ilmenite at high pressures, *Am. Mineral.*, *85*, 317.

Karki, B. B., R. M. Wentzcovitch, S. d. Gironcoli, and S. Baroni (2000b), Ab initio lattice dynamics of $MgSiO_3$ perovskite at high pressure, *Phys. Rev. B*, *62*(22), 14,750.

Karki, B. B., R. M. Wentzcovitch, S. d. Gironcoli, and S. Baroni (2000c), High pressure lattice dynamics and thermoelasticity of MgO, *Phys. Rev. B*, *61*(13), 8793.

Lam, P. K., R. Yu, L. M. W., and S. K. Sharma (1990), Structure distortion and vibrational modes in Mg2Si04, *Am. Mineral.*, *75*, 109–119.

Li, B., G. D. Gwanmesia, and R. C. Liebermann (1996), Sound velocities of olivine and beta polymorphs of Mg2SiO4 at Earth's transition zone pressures, *Geophys. Res. Lett.*, *23*(17), 2259–2262.

Meng, Y., D. J. Weidner, G. D. Gwanmesia, R. C. Liebermann, M. T. Vaughan, Y. Wang, K. Leinenweber, R. E. Pacalo, A. Yeganeh-Haeri, and Y. Zhao (1993), In situ high P-T X ray diffraction studies on three polymorphs (alpha, beta, gamma) of Mg_2SiO_4, *J. Geophys. Res., [Solid Earth Planets]*, *98*(12), 22,199–22,207.

Pavese, A. (1998), Thermoelastic and structural properties of forsterite as a function of P and T: A computer simulation study, by semi-classical potentials, *Phys. Chem. Miner.*, *26*(1), 44–54.

Perdew, J. P., and A. Zunger (1981), Self-interaction correction to density-functional approximations for many-electron systems, *Phys. Rev. B*, *23*, 5048.

Pilati, T., F. Demartin, and C. M. Gramaccioli (1995), Thermal parameters of minerals of the olivine group: Their implication on vibrational spectra, thermodynamic functions and transferable force fields, *Acta Crystallogr.*, *B51*, 721–733.

Price, G. D., S. C. Parker, and M. Leslie (1987), The lattice dynamics of forstertie, *Mineral. Mag.*, *51*, 157–170.

Rao, K., S. L. Chaplot, N. Choudury, S. Ghose, J. M. Hastings, and L. M. Corliss (1988), Lattice dynamics and inelastic neutron scattering from forsterite, Mg2SiO4: Phonon dispersion relation, density of states, and specific heat, *Phys. Chem. Miner.*, *16*, 83–97.

Stacey, F. D., and D. G. Isaak (2003), Anharmonicity in mineral physics: A physical interpretation, *J. Geophys. Res., [Solid Earth]*, *108*(B9).

Suzuki, I., H. Takei, and O. L. Anderson (1984), Thermal expansion of forsterite, Mg_2SiO_4, in *Thermal Expansion 8*, edited by H.T.A., pp. 79–88, Springer, New York.

Troullier, N., and J. L. Martins (1991), Efficient pseudopotential for plan wave calculations, *Phys. Rev. B*, *43*, 1993–2006.

Tsuchiy, T., J. Tsuchiya, K. Umemoto, and R. M. Wentzcovitch (2004), Elasticity of post-perovskite $MgSiO_3$, *Geophys. Res. Lett.*, *31*(14), L14603, doi:10.1029/2004GL020278.

Tsuchiya, J., T. Tsuchiya, and R. M. Wentzcovitch (2005), Vibrational and thermodynamic properties of MgSiO3 post-perovskite, *J. Geophys. Res.*, *110*, B02204, doi:10.1029/2004JB003409.

Wang, S. Y., S. K. Sharma, and T. F. Cooney (1993), Micro-Raman and infrared spectral study of forsterite under high pressure, *Am. Mineral.*, *78*(5–6), 469–476.

Wentzcovitch, R. M., and G. D. Price (1996), High pressure studies of mantle minerals by ab initio variable cell shape molecular dynamics, in *Molecular Engineering*, edited by B. Silvi, , and P. Darco, Springer, New York.

Wentzcovitch, R. M., and L. Stixrude (1997), Crystal chemistry of forsterite; a first-principles study, *Am. Mineral.*, *82*(7–8), 663–671.

Wentzcovitch, R. M., N. L. Ross, and G. D. Price (1995), Ab initio study of $MgSiO_3$ and $CaSiO_3$ perovskites at lower-mantle pressures, *Phys. Earth Planet. Inter.*, *90*(1–2), 101–112.

Wentzcovitch, R. M., B. B. Karki, M. Cococcioni, and S. de Gironcoli (2004), Thermoelastic properties of $MgSiO_3$-perovskite: Insights on the nature of the Earth's lower mantle, *Phys. Rev. Lett.*, *92*, 018501.

Yu, Y., and R. Wentzcovitch (2006), Density functional study of vibrational and thermodynamic properties of ringwoodite, *J. Geophys. Res.*, *111*, BI2202, doi:10.1029/2006JB004282.

Zha, C. S., T. S. Duffy, R. T. Downs, H. K. Mao, and R. J. Hemley (1994), Sound velocity and elasticity of single-crystal forsterite to 16 GPa, *J. Geophys. Res.*, *101*, 17,535–17,546.

L. Li and D. J. Weidner, Department of Geosciences, Mineral Physics Institute, Stony Brook University, Stony Brook, NY 11790, USA. (lilli@ic.sunysb.edu)

C. R. S. Da Silva and R. M. Wentzcovitch, Department of Chemical Engineering and Materials Science, Minnesota Supercomputing Institute for Digital Technology and Advanced Computations, University of Minnesota, 421 Washington Avenue SE, Minneapolis, MN 55455, USA.

JOURNAL OF GEOPHYSICAL RESEARCH, VOL. 113, B04206, doi:10.1029/2007JB005532, 2008

Correction to “Vibrational and thermodynamic properties of forsterite at mantle conditions”

Li Li, Renata M. Wentzcovitch, Donald J. Weidner, and Cesar R. S. Da Silva

Received 29 November 2007; published 17 April 2008.

Citation: Li, L., R. M. Wentzcovitch, D. J. Weidner, and C. R. S. Da Silva (2008), Correction to ‘‘Vibrational and thermodynamic properties of forsterite at mantle conditions,’’ *J. Geophys. Res.*, *113*, B04206, doi:10.1029/2007JB005532.

[1] In the paper “Vibrational and thermodynamic properties of forsterite at mantle conditions” by Li Li, Renata M. Wentzcovitch, Donald J. Weidner, and Cesar R. S. Da Silva (*Journal of Geophysical Research*, *112*, B05206, doi:10.1029/2006JB004546, 2007), Figure 3 was misdrafted. As a result, the region below 760 K is marked invalid for quasi-harmonic approximation (QHA). But this error does not alter the results nor the interpretation of the paper for the Earth since the geotherm is within the QHA valid region. Figure 3 is redrawn.

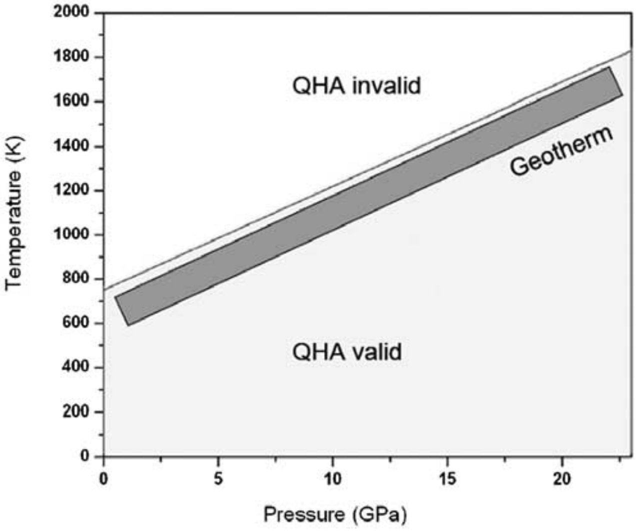

Figure 3. The valid pressure and temperature region of QHA estimated from calculated thermal expansion coefficient. The thick line indicates an estimate of geotherm [*Brown and Shankland*, 1981; *Green et al.*, 1999]; the light gray region is the QHA valid region.

0148-0227/08/2007JB005532$09.00